Inorganica Chimica Acta, 109 (1985) 105–110

Coordination Geometry and Structural Determinations of $SmPO_4$, $EuPO_4$ and $GdPO_4$

D. F. MULLICA, DAVID A. GROSSIE

Departments of Chemistry and Physics, Baylor University, Waco, Tex. 76798, U.S.A.

and L. A. BOATNER

Solid State Division, Oak Ridge National Laboratory, Oak Ridge, Tenn. 37831, U.S.A.*

Received September 11, 1984

Abstract

$SmPO_4$, $EuPO_4$, and $GdPO_4$ crystallize in the monoclinic system conforming to space group $P2_1/n$ (No. 14, $Z = 4$). The structures and coordination geometries of these three lanthanide orthophosphates have been determined by means of automated three-dimensional single crystal diffractometry using Mo Kα radiation. The lattice parameters of the three compounds are as follows: For $SmPO_4$, a = 6.669(1), b = 6.868(2), c = 6.351(1) Å, and β = 103.92(2)°; for $EuPO_4$, a = 6.639(3), b = 6.823(3), c = 6.318(3) Å and β = 104.00(4)°; and for $GdPO_4$, a = 6.621(2), b = 6.823(2), c = 6.310(2) Å, and β = 104.16(2)°. Final full-matrix least-squares refinements resulted in the following residual indices for $SmPO_4$, $EuPO_4$, and $GdPO_4$, respectively: R = 0.034, 0.033, and 0.031 and R_w = 0.034, 0.033, and 0.032. These results were based on 1103, 751, and 1073 reflections, respectively, for the three systems. The lanthanide atoms in this structure are coordinated to nine oxygen atoms forming a polyhedron, which has been described as a pentagonal interpenetrating tetrahedron. Important bond and contact distances and bond angles are presented along with ORTEP-II drawings that illustrate the coordination geometry.

Introduction

The lanthanide orthophosphates exhibit a combination of characteristics that has led to recent interest in the potential application of these materials as a primary encapsulation medium for the permanent disposal of certain types of radioactive wastes [1–3]. Characteristics of the lanthanide orthophosphates pertinent to an application of this type include the following: Both uranium and thorium have been contained in naturally occurring lanthanide orthophosphates (*i.e.*, monazite ores) for geological time periods. Additionally, recent evidence indicates that these substances readily recover from the type of heavy particle radiation damage to which a waste form containing alpha-active isotopes would be subjected. Finally, orthophosphates whose crystal structure is the same as that of the lanthanide orthophosphates in the first half of the transition series can be formed from many of the actinides produced by nuclear reactor operation. The latter characteristic suggests that, in some cases, it may be possible to match the crystal chemistry of the radioactive actinide species to that of the host nuclear waste form.

The potentially important application of lanthanide orthophosphates to nuclear waste disposal has led to increased interest in their fundamental physical and chemical properties; and recent work in this area has included investigations of valence states and site symmetries of actinide, iron group, and rare-earth impurities [4–7], as well as studies employing Raman scattering [8], optical absorption spectroscopy [9–11] and Rutherford backscattering [3]. Structurally, the pure lanthanide orthophosphates may be divided into two classes. Elements in the second half of the transition series from Tb to Lu form orthophosphates with a tetragonal zircon structure, while the elements in the first half of the series from La to Gd crystallize with the monoclinic 'monazite' structure. We have previously reported the results of single crystal X-ray structural refinements for all of the tetragonal orthophosphates plus the related materials YPO_4 and $ScPO_4$ and have also carried out structural investigations on the monoclinic phosphates $LaPO_4$ and $CePO_4$ [12–16]. In the present work, as part of our continuing effort to study the crystal chemistry of the entire series of lanthanide orthophosphates, we report the results

*Operated by Martin Marietta Energy Systems, Inc. under contract DE-AC05-840R21400 with the U.S. Department of Energy.

0020-1693/85/$3.30

of structural investigations for crystals of $SmPO_4$, $EuPO_4$, and $GdPO_4$.

Experimental

A high-temperature flux technique described previously [17, 18] was employed in growing single crystals of the subject orthophosphates. Single crystal specimens of Sm, Eu, and $GdPO_4$, selected on the basis of their optical quality, were ground using a Nonius crystal grinder. (The crystal radii in cm were 0.0219, 0.0273, and 0.0219, respectively, for Sm, Eu, and $GdPO_4$.) X-ray measurements were made using an Enraf-Nonius CAD-4F diffractometer (Mo K_α, λ_{mean} = 0.71073 Å) equipped with an Ortec series 7000 Si(Li) solid-state detector system which permitted routine fluorescence analysis. The metal constituents were initially qualitatively verified. Cell dimensions and a working orientation matrix for each compound were obtained from 25 carefully centered reflections using a least-squares refinement routine associated with the diffractometer (see Table I). Intensity data from the spherically ground crystals were measured by the $\omega - 2\theta$ scan technique at a rate of 0.38–3.35° min^{-1}, determined by a fast prescan of 3.35° min^{-1}. A variable scan width was selected according to A + B tan θ (see Table I for A and B values). Reflections having <75 counts above background during the prescan were assumed to be unobserved. Two check reflections in each data set were examined after every 2 h of exposure time in order to verify the stability of the X-ray intensity measurements and the reliability of the electronics. Intensities of all standards did not vary appreciably during the data collections. The respective mean disagreement factor was <1.5% from the average value for each monitored reflection in each data set. All diffraction data were corrected for Lorentz and polarization factors as well as for absorption effects (μR = 4.65, 6.25, 5.37, for Sm, Eu, and $GdPO_4$). After averaging, all unique reflections having $I_{rel} > 3\sigma$ (I_{rel}) were used in the solution and refinement of the structures. The experimental conditions and statistical summaries are also listed in Table I.

Structural Refinement

Systematic extinctions ($h0l$, $h + l = 2n + 1$ and $0k0$, $k = 2n + 1$) validated the space group assignment $P2_1/n$. Initial starting atomic parameters were taken from the structural analysis of the analog compound $CePO_4$ [14]. The model was initially refined isotropically for each set of data using a full-matrix least-squares refinement program obtained from Enraf-Nonius [19]. Anisotropic thermal parameters and secondary extinction corrections (g) were applied in the final refinement stages. The

TABLE I. Experimental and Statistical Summaries.

		$SmPO_4$	$EuPO_4$	$GdPO_4$
a (Å)		6.669(1)	6.639(3)	6.621(2)
b		6.868(2)	6.823(3)	6.823(2)
c		6.351(1)	6.318(3)	6.310(2)
β		103.92(2)	104.00(4)	104.16(2)
V (Å^3)		282.4(2)	277.7(3)	276.4(4)
Space group		$P2_1/n$	$P2_1/n$	$P2_1/n$
MW.		245.32	246.93	252.22
$F(000)$		436	440	444
D (Mg m^{-3})		5.771	5.876	6.061
Crystal radius (cm)		0.0219	0.0273	0.0219
μ (MoK_α) mm^{-1}		21.25	22.88	24.50
$\Delta\omega$ (°) ($\omega - 2\theta$ scan)		1.25 + 0.35 tan θ	1.25 + 0.35 tan θ	1.30 + 0.35 tan θ
$\Delta\theta$ (°)		1.5–35.0	1.5–30.0	1.5–35.0
Scan limits (° min^{-1})		0.38–3.35	0.38–3.35	0.38–3.35
Transmission factor range		0.008–0.031	0.003–0.016	0.005–0.027
Unique refl.		1103	751	1073
Systematic absences		$h0l$, $h + l = 2n + 1$	$h0l$, $h + l = 2n + 1$	$h0l$, $h + l = 2n + 1$
		$0k0$, $k = 2n + 1$	$0k0$, $k = 2n + 1$	$0k0$, $k = 2n + 1$
R		0.034	0.033	0.031
Rw		0.034	0.033	0.032
GnFt(Σ_2)		1.90	2.17	1.66
g (e^{-2}) (10^{-6})		2.34(3)	2.12(3)	1.82(3)
Max [$\Delta\xi i/\sigma(\xi i)$] ($10^{-4}$)		9.5	7.8	7.5
Residual (e Å^{-3})	max.	2.6(6)	2.3(5)	4.1(5)
	min.	−3.3(6)	−3.6(5)	−3.6(5)

completed structural refinement provided final respective residual index factors $R = \Sigma\Delta F/\Sigma|F_o| = 0.034, 0.033, 0.031$, and $R_w = [\Sigma w(\Delta F)^2/\Sigma w(F_o)^2]^{1/2} = 0.034, 0.033, 0.032$ where $\Delta F = ||F_o| - |F_c||$ and the reciprocal of the square of the standard deviation on F_o, $\sigma^{-2}(F_o)$, defines the weighting factor, w. The 'goodness of fit' values (Gnft) related to each data set were reasonable $\Sigma_2 = 1.90, 2.17$, and 1.66 for Sm, Eu, and $GdPO_4$, respectively, where Gnft is expressed as $\Sigma_2 = [\Sigma w(\Delta F)^2/(N_o - N_v)]^{1/2}$. Here N_o and N_v are, respectively, the number of independent observations and varied parameters in the least-squares refinement. The maximum abscission values ($[\Delta\xi_i/(\xi_i)]$ where ξ_i values are varied parameters) obtained from the final cyclic process for each refinement are also presented in Table I along with the maximum and minimum residual densities found in the vicinity of the lanthanide metals on final difference Fourier maps. Elsewhere, only random undulating background was observed. Scattering factors with related anomalous dispersion correction factors for each atom were obtained from the work of Ibers and Hamilton [20]. Tables II and III list the final atomic positional parameters with equivalent isotropic thermal parameters and anisotropic thermal parameters with estimated standard deviations (e.s.d.s) in parentheses for samarium, europium, and gadolinium orthophosphate.

Discussion

The experimental bond and contact distances and bond angles for samarium, europium, and gadolinium orthophosphate are presented in Table IV. The phosphate group in each compound is a distorted tetrahedron as evidenced by deviations from the norm of O–P–O angles, even though the average phosphorus–oxygen distance in each structure is in excellent agreement with P–O bond distances found in BIDICS [21]. The experimental bond lengths are also internally consistent when considering the summation of the atomic radii of the bonding atoms. The effective ionic radii of Sm, Eu, Gd, were obtained from the work of Shannon [22]. The calculated bond lengths obtained from the summation of the effective ionic radii are Sm–,Eu–, and Gd–O = 2.492, 2.480, and 2.467 Å, respectively, and P–O = 1.53 Å. The method for determining effective ionic radii assumes that even though individual cation-anion bond lengths vary within a polyhedron, the average cation-anion distance over all similar polyhedra in *one structure* is constant [22] and, therefore, it is proper to compare calculated bond distances to averaged experimental bond distances. The respective calculated-experimental bond differences between the P–O, Sm–O, Eu–O, and Gd–O distances are, respectively, 0.00, 0.001, 0.005, and 0.006 (0.0, 0.04, 0.20, and 0.24% variance).

TABLE II. Positional Parameters (×10⁴) and Equivalent Isotropic Thermal Parameters (×10⁴) for Samarium, Europium and Gadolinium Orthophosphate.

	Atom	*x*	*y*	*z*	U_{eq}[a]
$SmPO_4$	Sm[b]	28164(5)	15645(5)	9823(5)	20(5)
	P	3031(2)	1619(2)	6129(3)	17(3)
	O(1)	2503(8)	29(8)	4402(8)	60(9)
	O(2)	3837(7)	3337(8)	5014(8)	56(9)
	O(3)	4742(8)	1030(8)	8099(8)	67(9)
	O(4)	1223(7)	2120(8)	7119(8)	54(9)
$EuPO_4$	Eu[b]	28160(5)	15580(6)	9758(6)	22(1)
	P	3030(3)	1616(3)	6131(3)	25(4)
	O(1)	2508(9)	19(9)	4393(10)	68(10)
	O(2)	3829(9)	3337(9)	5006(10)	56(12)
	O(3)	4731(9)	1025(10)	8116(10)	67(13)
	O(4)	1200(9)	2125(9)	7125(10)	52(12)
$GdPO_4$	Gd[b]	28152(4)	15535(4)	9694(5)	58(1)
	P	3026(2)	1615(3)	6133(3)	59(3)
	O(1)	2532(8)	7(8)	4392(8)	113(10)
	O(2)	3829(7)	3348(8)	5019(8)	99(9)
	O(3)	4727(8)	1017(8)	8129(8)	105(10)
	O(4)	1203(7)	2113(8)	7126(8)	99(9)

[a]U_{eq} defined as one third the trace of the orthogonalized U_{ij} tensor. [b]Coordinates ×10⁵.

TABLE III. Anisotropic Thermal Parameters ($\times 10^4$) for Samarium, Europium and Gadolinium Orthophosphate.

Name	U_{11}	U_{22}	U_{33}	U_{12}	U_{13}	U_{23}
$SmPO_4$						
Sm	20(1)	13(1)	44(1)	1(1)	39(1)	7(1)
P	17(5)	5(5)	49(5)	2(5)	47(4)	3(5)
O(1)	70(19)	43(19)	70(17)	15(15)	18(14)	16(15)
O(2)	54(15)	39(18)	107(16)	−8(15)	81(12)	21(16)
O(3)	44(16)	102(20)	63(17)	29(16)	26(14)	8(17)
O(4)	53(15)	42(17)	88(17)	58(15)	58(13)	17(16)
$EuPO_4$						
Eu	−18(1)	27(2)	61(2)	0(1)	14(1)	6(1)
P	−20(7)	39(8)	60(8)	2(6)	11(6)	4(7)
O(1)	38(22)	48(26)	94(25)	−2(21)	−30(20)	13(21)
O(2)	13(20)	64(25)	102(23)	−19(20)	36(17)	39(21)
O(3)	21(21)	104(27)	73(23)	23(21)	9(18)	6(22)
O(4)	20(20)	45(23)	105(23)	31(20)	43(17)	−13(22)
$GdPO_4$						
Gd	27(1)	50(1)	93(1)	2(1)	8(1)	7(1)
P	26(5)	57(6)	93(5)	−3(5)	10(4)	0(5)
O(1)	95(18)	90(19)	134(19)	40(16)	−12(15)	−4(16)
O(2)	60(15)	92(18)	162(17)	−19(15)	58(13)	27(16)
O(3)	71(17)	119(19)	116(17)	45(16)	8(14)	−7(16)
O(4)	56(16)	76(17)	170(18)	60(15)	42(13)	24(16)

The form of the anisotropic thermal parameter is: $\exp[-2\pi^2\{h^2a^{*2}U_{11} + k^2b^{*2}U_{22} + l^2c^{*2}U_{33} + 2hka^*b^*U_{12} + 2hla^*c^*U_{13} + 2klb^*c^*U_{23}\}]$.

TABLE IV. Bond Distances (Å) and Angles (°) for Samarium, Europium and Gadolinium Orthophosphate.

	$SmPO_4$	$EuPO_4$	$GdPO_4$
Ln–O(1)	2.468(4)	2.453(4)	2.452(4)
	2.396(4)	2.378(4)	2.373(4)
Ln–O(2)	2.577(4)	2.570(4)	2.560(4)
	2.489(4)	2.466(4)	2.453(4)
	2.768(4)	2.753(4)	2.764(4)
Ln–O(3)	2.504(4)	2.475(4)	2.461(4)
	2.390(4)	2.374(4)	2.365(4)
Ln–O(4)	2.458(4)	2.441(4)	2.429(4)
	2.389(4)	2.365(4)	2.364(4)
Avg.	2.493	2.475	2.469
O(1)–O(2)	2.437(5)	2.425(6)	2.434(6)
O(1)–O(3)	2.555(5)	2.550(6)	2.544(6)
O(1)–O(4)	2.546(5)	2.552(6)	2.561(6)
O(2)–O(3)	2.479(5)	2.477(6)	2.482(6)
O(2)–O(4)	2.578(5)	2.579(6)	2.575(5)
O(3)–O(4)	2.399(5)	2.396(6)	2.384(5)
P–O(1)	1.528(4)	1.526(5)	1.531(4)
P–O(2)	1.538(4)	1.532(4)	1.535(4)
P–O(3)	1.531(4)	1.525(4)	1.526(4)
P–O(4)	1.527(4)	1.537(4)	1.528(4)
Avg.	1.531	1.530	1.530

TABLE IV *(continued)*

	$SmPO_4$	$EuPO_4$	$GdPO_4$
O(1)–P–O(2)	105.3(2)	104.9(3)	105.1(2)
O(1)–P–O(3)	113.3(2)	113.4(3)	112.7(2)
O(1)–P–O(4)	112.8(2)	113.0(2)	113.7(2)
O(2)–P–O(3)	107.7(2)	108.3(3)	108.4(2)
O(2)–P–O(4)	114.5(2)	114.4(3)	114.4(2)
O(3)–P–O(4)	103.3(2)	103.0(2)	102.6(2)
Avg.	109.5	109.5	109.5

A more detailed discussion describing the 9-coordinated geometry of $SmPO_4$, $EuPO_4$, and $GdPO_4$ can be found elsewhere [12]. The ninefold coordination in monoclinic ($P2_1/n$) lanthanide (Ln) orthophosphates is best described as a pentagonal interpenetrating tetrahedral polyhedron (PITP). Figure 1 is a representative ORTEP II stereoview of $LnPO_4$. The point group symbol is C_s, a plane of symmetry. This is shown in Fig. 2(a) for a representative $LnPO_4$; and in Fig. 2(b), an idealized PITP geometry is presented for comparative purposes. In these monazite analogue structures (MXO_4), the metal lanthanide (Ln) atoms are La, Ce, Pr, Nd, Sm, Eu,

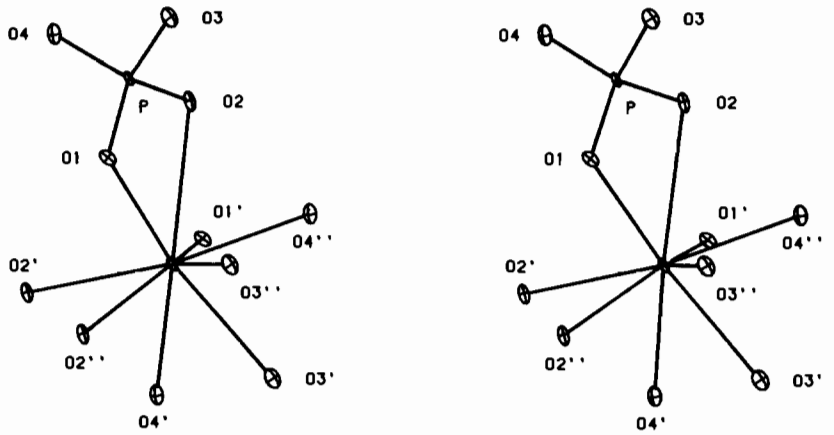

Fig. 1. Stereoview of the 9-coordinated geometry associated with monoclinic $LnPO_4$ compounds ($P2_1/n$) with the labeling and numbering scheme—PITP (pentagonal interpenetrating tetrahedral polyhedron).

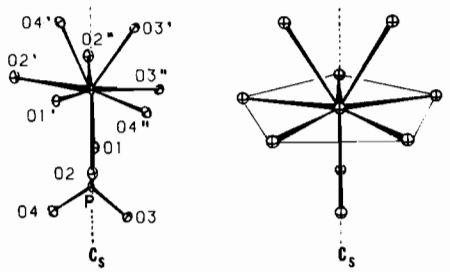

(a) (b)

Fig. 2. (a) $LnPO_4$ coordination group showing C_s symmetry. (b) Idealized PITP (pentagonal interpenetrating tetrahedral polyhedron) demonstrating the plane of symmetry, C_s.

and Gd, and X is a phosphorus but could conceivably be either vanadium or arsenic. Considering only the atoms defining the pentagonal planes in $LnPO_4$ compounds, a least-squares planarity calculation [23] yielded the conclusion that planarity exists with some distortion. The weighted mean distances related to the pentagonal planes of each analyzed structure (Sm, Eu, and $GdPO_4$) are 0.132, 0.129, and 0.131 Å, respectively. The rigid geometry associated with the pentagonal interpenetrating tetrahedral polyhedron is attributed to the bidentate bonding of the tetrahedral phosphate groups. The 9-coordinated Ln atoms are apically linked together in a chain-like fashion by very slightly distorted tetrahedral phosphate groups. Figure 3 illustrates this chain-like linkage. The apical bidentate bonding accounts for four of the nine oxygen atoms in PITP. The remaining five oxygen atoms form the equatorial pentagonal plane. These oxygen atoms are locked in position via bridging to five surrounding strands of chain-like linkage, *i.e.*, the bridging provides a locking effect which supports and secures the pentagonal plane. For clarity, Fig. 3 shows only two of the five surrounding strands forming the interlocking mechanism. In the lower right portion of the stereoview in Fig. 3, the ninefold geometry of monoclinic ($P2_1/n$) lanthanide orthophosphate compounds (with small filled oxygen atoms) can be seen as well as the two centrally located 9-coordinated Ln atoms elucidating the locking mechanism. Future experimental work as well as an examination of previously published results is expected to reveal many more examples of this new ninefold coordination geometry (PITP). In fact, as mentioned in our earlier work [12], Rice and Robinson [24], using single crystal X-ray diffractometry, have shown that La in $LaVO_4$ is 9-coordinated and not 8-coordinated. The nona-coordination polyhedron observed in their work [24] was classified as an irregular polyhedron containing a pentagonal plane with two oxygen atoms above the plane and two oxygen atoms below the plane. A construction of a scale model of $LaVO_4$ using a Supper Model Builder established that $LaVO_4$ has the same type 9-coordinated geometry as $LnPO_4$, *i.e.*, a pentagonal interpenetrating tetrahedral polyhedron (PITP).

Structural refinements of the monoclinic orthophosphates $PrPO_4$ and $NdPO_4$ are currently in progress, and these results will be reported elsewhere. With the addition of these two structures to the present results and our previously reported work, refinements for the entire transition series as well as YPO_4 and $ScPO_4$ will have been completed. These results form the basis for following the transition from the monoclinic monazite structure to the tetragonal zircon structure as the lanthanide contraction occurs in going to the heavier rare earths. Additionally, these findings are central to ongoing studies of heavy particle radiation effects and alteration effects in the lanthanide orthophosphates that are potential hosts for the permanent disposal of actinide (and other) radioactive wastes.

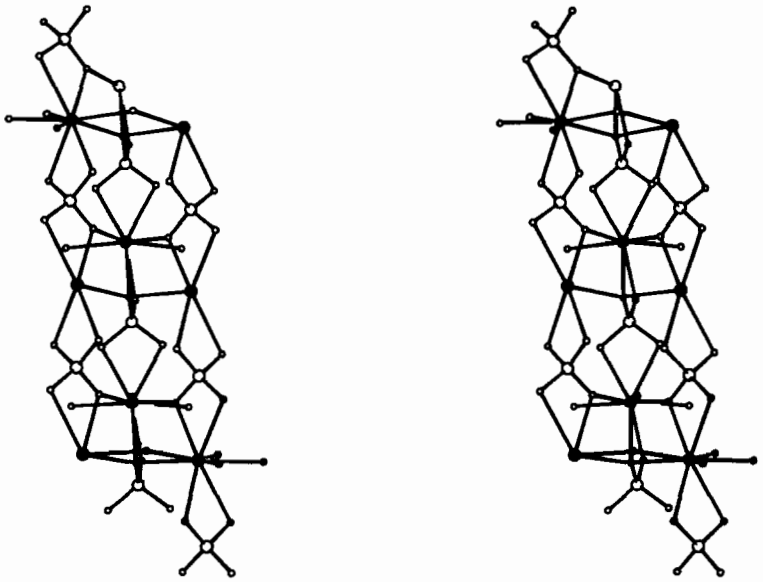

Fig. 3. Monoclinic $LnPO_4$—a stereoscopic drawing shows the interlocking mechanism of the chain-like strands. The large solid circles represent lanthanide elements, while the large open circles are phosphorus atoms, and the small open circles are oxygen atoms).

Acknowledgements

This investigation was supported in part by The Robert A. Welch Foundation (Grant No. AA-668) and Baylor University.

We wish to further express our gratitude and reverence to our departed friend Dr. W. O. Milligan who rendered assistance and support to this project.

References

1 L. A. Boatner, G. W. Beall, M. M. Abraham, C. B. Finch, P. G. Huray and M. Rappaz, in C. J. Northrup (ed.), 'Scientific Basis for Nuclear Waste Management, Vol. 2', Plenum, New York, 1980, p. 289.
2 L. A. Boatner, G. W. Beall, M. M. Abraham, C. B. Finch, R. J. Floran, P. G. Huray and M. Rappaz, 'Management of Alpha-Contaminated Wastes', IAEA-SM-246/73, International Atomic Energy Agency, Vienna, 1981, p. 411.
3 B. C. Sales, C. W. White and L. A. Boatner, *Nucl. Chem. Waste Manage., 4* (1984) in press.
4 M. M. Abraham and L. A. Boatner, *Phys. Rev. B, 26*, 1434 (1982).
5 M. Rappaz, M. M. Abraham, J. O. Ramey and L. A. Boatner, *Phys. Rev. B, 23*, 1012 (1981).
6 M. M. Abraham, L. A. Boatner, J. O. Ramey and M. Rappaz, *J. Chem. Phys., 78*, 3 (1983).
7 K. L. Kelley, G. W. Beall, J. P. Young and L. A. Boatner, in J. G. Moore (ed.), 'Scientific Basis for Nuclear Waste Management, Vol. 3', Plenum, New York, 1981, p. 189.
8 G. M. Begun, G. W. Beall, L. A. Boatner and W. T. Gregor, *J. Raman Spectrosc., 11*, 273 (1981).
9 T. Hayhurst, S. Shalimoff, N. Edelstein, L. A. Boatner and M. M. Abraham, *J. Chem. Phys., 74*, 5449 (1981).
10 T. Hayhurst, S. Shalimoff, J. G. Conway, N. Edelstein, L. A. Boatner and M. M. Abraham, *J. Chem. Phys., 76*, 3960 (1982).
11 P. C. Becker, T. Hayhurst, G. Shalimoff, J. G. Conway, L. A. Boatner and M. M. Abraham, *J. Chem. Phys.*, in press.
12 D. F. Mullica, W. O. Milligan, David A. Grossie, G. W. Beall and L. A. Boatner, *Inorg. Chim. Acta, 95*, 231 (1984).
13 W. O. Milligan, D. F. Mullica, G. W. Beall and L. A. Boatner, *Inorg. Chim. Acta, 60*, 39 (1982).
14 G. W. Beall, L. A. Boatner, D. F. Mullica and W. O. Milligan, *J. Inorg. Nucl. Chem., 43*, 101 (1981).
15 W. O. Milligan, D. F. Mullica, G. W. Beall and L. A. Boatner, *Acta Crystallogr., Sect. C:, 39*, 23 (1983).
16 W. O. Milligan, D. F. Mullica, G. W. Beall and L. A. Boatner, *Inorg. Chim. Acta, 70*, 133 (1983).
17 R. S. Feigelson, *J. Am. Ceram. Soc., 47*, 257 (1964).
18 M. Rappaz, J. O. Ramey, L. A. Boatner and M. M. Abraham, *J. Chem. Phys., 76*(1), 40 (1982).
19 Enraf-Nonius, 'ENRAF-NONIUS VAX', Structure Determination Package, Delft, Holland, 1982.
20 J. A. Ibers and W. C. Hamilton (eds.), 'International Tables for X-Ray Crystallography, Vol. IV', Kynoch Press, Birmingham, 1974, p. 72.
21 'Bond Index of the Determination of Inorganic Crystal Structures', BIDICS, Institute for Material Research, Hamilton, Canada, 1969–1981.
22 R. D. Shannon, *Acta Crystallogr., Sect. A:, 32*, 751 (1976).
23 D. M. Blow, *Acta Crystallogr., 13*, 168 (1960).
24 C. E. Rice and W. R. Robinson, *Acta Crystallogr., Sect. B:, 32*, 2232 (1976).